The Journal of Experimental Biology 216, 4222-4232

doi:10.1242/jeb.085209

RESEARCH ARTICLE

Experimental verification of dynamic soaring in albatrosses

G. Sachs[1,*], J. Traugott[1], A. P. Nesterova[2] and F. Bonadonna[2]

[1]Institute of Flight System Dynamics, Technische Universität München, Boltzmannstrasse 15, 85748 Garching, Germany and
[2]Behavioural Ecology Group, Centre d'Ecologie Fonctionnelle et Evolutive, U.M.R., 5175 CNRS Montpellier, France

*Author for correspondence (sachs@tum.de)

SUMMARY

Dynamic soaring is a small-scale flight manoeuvre which is the basis for the extreme flight performance of albatrosses and other large seabirds to travel huge distances in sustained non-flapping flight. As experimental data with sufficient resolution of these small-scale movements are not available, knowledge is lacking about dynamic soaring and the physical mechanism of the energy gain of the bird from the wind. With new in-house developments of GPS logging units for recording raw phase observations and of a dedicated mathematical method for postprocessing these measurements, it was possible to determine the small-scale flight manoeuvre with the required high precision. Experimental results from tracking 16 wandering albatrosses (*Diomedea exulans*) in the southern Indian Ocean show the characteristic pattern of dynamic soaring. This pattern consists of four flight phases comprising a windward climb, an upper curve, a leeward descent and a lower curve, which are continually repeated. It is shown that the primary energy gain from the shear wind is attained in the upper curve where the bird changes the flight direction from windward to leeward. As a result, the upper curve is the characteristic flight phase of dynamic soaring for achieving the energy gain necessary for sustained non-flapping flight.

Key words: non-flapping flight, energy gain from wind, GPS logger, shear wind.

Received 14 January 2013; Accepted 5 August 2013

INTRODUCTION

Albatrosses excel in an extreme travelling performance by covering huge distances in their foraging trips with sustained non-flapping flight. Flight recordings show distances of thousands of kilometres as well as flights around the world in 46 days (Jouventin and Weimerskirch, 1990; Bonadonna et al., 2005; Croxall et al., 2005). Furthermore, albatrosses are able to fly persistently at high speed by using favourable winds (Catry et al., 2004).

The reason for this unique performance capability is a flight mode termed dynamic soaring. With dynamic soaring, the birds achieve an energy gain from the shear wind above the ocean surface, enabling sustained non-flapping flight. As a result, the birds can fly at virtually no cost when compared with flapping flight (Weimerskirch et al., 2000). By applying dynamic soaring (Sachs, 2005; Sachs et al., 2012), the birds gain access to an unlimited external energy source in terms of the shear wind above the sea surface. The unique advantage of having an unlimited energy source is due to the fact that there are permanently strong winds in the areas in which albatrosses live (Suryan et al., 2008). These brief considerations show that dynamic soaring is fundamental for the extreme travelling performance of albatrosses, enabling their unique way of flying and living.

The long distance flight of albatrosses, constituting a large-scale movement of the order of hundreds to thousands of kilometres, has been experimentally investigated at great length and is well documented (Jouventin and Weimerskirch, 1990; Weimerskirch et al., 2000; Weimerskirch et al., 2002; Catry et al., 2004; Bonadonna et al., 2005; Croxall et al., 2005). By contrast, the dynamic soaring flight mode of albatrosses and other large seabirds has not been experimentally investigated. This is because dynamic soaring is a small-scale movement of the order of tens to hundreds of metres (Sachs, 2005).

A primary goal of this paper is to advance the knowledge in the field of dynamic soaring in albatrosses and their unique flight method of gaining energy from the wind for flying without flapping. The current state of knowledge manifests in a variety of theories and explanations for the small-scale dynamic soaring flight of albatrosses. There is a theory termed wind-gradient soaring (Lighthill, 1975; Norberg, 1990; Spedding, 1992; Tickell, 2000; Dhawan, 2002; Lindhe Norberg, 2004; Azuma, 2006; Denny, 2009); according to this theory, soaring is continually possible using the wind gradient in the shear layer above the sea surface. Another theory termed gust soaring relates to discontinuities in the wind flow (Pennycuick, 2002; Pennycuick, 2008; Suryan et al., 2008; Langelaan, 2008; Langelaan and Bramesfeld, 2008); according to this theory, energy pulses are obtained from flight through the separated air flow region behind wave crests. Furthermore, wave soaring and wave lift are regarded as a technique to obtain energy for flying (Berger and Göhde, 1965; Wilson, 1975; Pennycuick, 1982; Sheng et al., 2005; Richardson, 2011); here, updrafts at waves are supposed to be usable for soaring. Another point relates to the aerodynamic ground effect (Blake, 1983; Hainsworth, 1988; Norberg, 1990; Rayner, 1991); this effect yields a decrease of the drag when flying close to the water surface so that an energetic advantage is possible at low levels.

To sum up, current theories and explanations are differing and show various findings and conclusions. As a result, there is a lack of both knowledge of dynamic soaring and clarity about this flight mode, particularly with regard to the magnitude of the achievable energy gain and the physical transfer mechanism of energy from the wind to the bird. This is due to the fact that there are so far no

experimental data of the small-scale movements of albatrosses so that a full understanding of dynamic soaring could not be achieved.

To address the aims of this paper, in-flight measurements of the small-scale movements in free-flying birds were performed so that experimental verification of dynamic soaring in albatrosses could be accomplished. The experimental verification was achieved with new in-house developments of appropriate GPS logger hardware and of a novel mathematical method for computing the albatrosses' flight path and speed with the high precision required for this small-scale flight mode.

MATERIALS AND METHODS

New in-house developments were accomplished in order to achieve the required high precision in determining the small-scale movements of dynamic soaring in albatrosses (Traugott et al., 2008a). One pertains to the hardware, yielding a miniaturized GPS logging unit for recording raw L1 phase measurements at high sampling rate. The other in-house development is a new mathematical method for determining the flight path and speed with high precision. The new in-house developments were tested for correct functioning prior to being used for the albatross flight measurements. These trials included test runs with a car as well as flight tests with several aeroplanes (Traugott et al., 2008a; Traugott et al., 2008b).

New logger hardware

Three different types of GPS data loggers were developed for the albatross flight measurements. The core of each device was a passive 25×25 mm patch antenna plugged to the single frequency GPS module LEA-4T (size 17×22.4 mm, mass 2.1 g; u-blox, Thalwil, Switzerland). This module is capable of calculating position and velocity online with a sampling rate of 4 Hz. When logging the data to the on-chip 8 MB flash memory or to an external memory this yields a data stream of 0.8 MB h^{-1}. As an additional feature, the LEA-4T module makes the GPS raw data available with a sampling rate of up to 10 Hz (~9.6 MB h^{-1}). These data are the basis for online positioning but can also be re-processed back for precision and sampling rate augmentation. Because of known issues when forcing the module to output both the online solution and the raw data at maximum rates, the online solution rate was limited to 1 Hz during the measurement campaign (210 kB h^{-1}). The average power consumption of the loggers was given by 40–60 mA and 2.9–3.7 V. Energy was provided by two or three 3.6 V primary lithium–thionyl chloride cells (Saft LS 14500 and LS 14500 C).

Two types of loggers featured an external 2 GB memory card. Equipped with three batteries, these devices were capable of logging the raw GPS data throughout a period of up to 6 days. Their form factor was 89×55×22 mm and 108×55×19 mm at a total mass of 103 and 93 g.

The third type of logger additionally featured a 3-axes MEMS accelerometer. No external memory was provided but all data were logged to the on-chip 8 MB flash which yielded possible recording intervals to about 40 min. For bridging the delay between mounting a logger on a bird at the nesting site and the bird finally cruising over open waters, these loggers implemented a reliable sleep/wake-up logic triggering high rate recording only when the bird had left a predefined area and was exceeding a given speed threshold.

In Fig. 1A, a miniaturized GPS data logger is shown. The complete logging unit includes the logger, the batteries, the wiring and the casing. The GPS logging unit was flight tested prior to being used for the albatross flight measurements. One of the aircraft used in the flight test programme is shown in Fig. 1B. This test vehicle

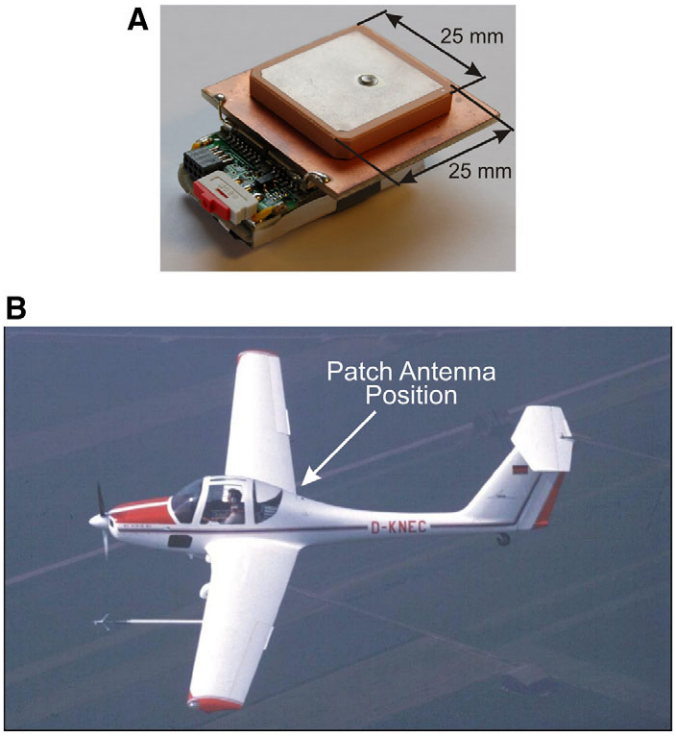

Fig. 1. GPS logger and research aircraft used in flight testing. (A) A miniaturized GPS data logger with an attached 25×25 mm patch antenna used in the albatross flight measurements is depicted. (B) The GPS logging unit, which includes the logger, the batteries, the wiring and the casing, was flight tested using several aircraft. The vehicle shown is a research aircraft of the Institute of Flight System Mechanics of the Technische Universität München.

is a research aircraft of the Institute of Flight System Mechanics of the Technische Universität München. The goal of the trials was to test the GPS data logger hardware as well as the new mathematical method for precise position determination. As no experience was on hand with regard to the required high position precision and high sampling rate, the development of the system involved significant test efforts. An issue of proper functioning for the planned albatross flight measurements was GPS signal shadowing at large bank angles, like the values occurring in dynamic-soaring-type flight manoeuvres of albatrosses. Therefore, the flight tests comprised, among others, dynamic manoeuvres with high bank angles to simulate those of dynamic soaring in albatrosses.

New mathematical method

A new mathematical method was developed to achieve relative position precision in the low decimetre range depending on environmental conditions. The high precision is obtained by forming single differences between raw L1 phase measurements taken by the moving receiver at two moments in time. Neither a second, nearby base receiver nor any (static) initialization procedures as commonly used in geodetic applications exploiting the same type of precise measurements are required by this differential GPS (D-GPS) approach. Details of the method are given elsewhere (Traugott et al., 2008a; Traugott et al., 2008b).

In Fig. 2, the basic concept of the approach for coping with the position determination task is graphically presented: in this exemplary scenario, a starting point is specified for an arbitrary time t_{b1} at the beginning of a flight manoeuvre of interest. The corresponding

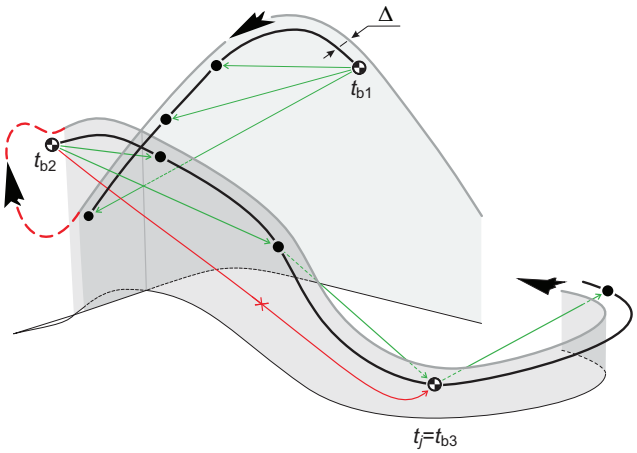

Fig. 2. Principle of time difference approach. $t_{b1–3}$, time base; t_j, current time; Δ, bias.

position of the vehicle is not known exactly but is estimated by techniques such as code-based single point positioning, a technique yielding robust, absolute position information limited to metre-level accuracy. Therefore, the start position is biased from the true location by Δ. The subsequent trajectory is now determined by time-differential processing relative to this starting point. In other terms, the base vectors pointing from the starting epoch to the current position are determined exactly. Hence, all fixes are afflicted by the same bias Δ. Phase measurements are sensible to signal shadowing – a short upside-down interlude can cause signal obstruction and prevent further processing. A new base at t_{b2} can be imported from the single point solution right after the manoeuvre (no re-initialization) and processing can be continued relative to the new base. Such an event causes a gap in the resulting trajectory. In the case shown in Fig. 2, the solution fails again between the base epoch t_{b2} and the current time t_j. However, this time there are enough healthy satellites observed at $t_{j–1}$ and t_j to calculate the baseline between these two points. A base hand-over preventing a gap in the solution can be realized and processing is hereupon continued to t_{b3}. A detailed description is given elsewhere (Traugott et al., 2008a; Traugott et al., 2008b).

The new mathematical method yields a position precision in the low decimetre region (Traugott et al., 2008a) so that an improvement in precision by a factor of 10 when compared with the state of the art is achieved. This holds for position precision in the longitudinal and lateral directions as well as in the vertical direction. In addition to this precision improvement, the position data are recorded at a sampling rate of 10 Hz, which is also significantly higher than the state of the art as regards comparable miniaturized devices.

Wind determination

Wind information was obtained using SeaWinds on QuikSCAT Level 3 Daily, Gridded Ocean Wind Vectors (JPL SeaWinds Project; winds.jpl.nasa.gov). The data are sampled on an ~0.25°×0.25° global grid twice a day (equal to 28 km in north–south direction and 18 km in east–west direction at 49° south). The data provide local wind velocity vectors at a reference altitude of 10 m with an accuracy of 2 m s^{-1} (or 10% for velocities above 20 m s^{-1}) and the wind direction within ±20°. Additional information is provided elsewhere (Perry, 2001).

For calculating the wind at the respective trajectory point, an in-house computational procedure was developed using one-dimensional linear interpolation in the time domain and bivariate Akima interpolation in the position domain (Müller, 2009).

Field work

The field work took place during a research stay of 3 months close to the Albatross colony at Cap Ratmanoff, Kerguelen Archipelago, southern Indian Ocean, on wandering albatrosses (*Diomedea exulans* Linnaeus 1758).

The miniaturized GPS logging units were taped to the back feathers of the birds using TESA tape according to the procedure suggested by Wilson et al. (Wilson et al., 1997). The mass of the miniaturized GPS logging units, which was 107 g in the heaviest version, represented about 1.0–1.3% of the mass of the birds, thus being less than 3% of the birds' mass as recommended by Phillips et al. (Phillips et al., 2003). The GPS units were recovered at the end of a foraging trip. Twenty GPS units were deployed, of which 16 provided high-quality flight data of the bird's trajectories. Two GPS units were damaged by saltwater, two others provided data from sitting birds that delayed their departure.

RESULTS AND DISCUSSION

Large-scale and small-scale movements

Reference is first made to the large-scale movement in terms of a foraging trip of an albatross to show a complete data recording of high-precision tracking at 10 Hz. In Fig. 3, the ground track of the flight that begins and ends at the Kerguelen Archipelago is presented. The overall duration of the trip was 3.2 days and its length was 1120 km.

A closer examination of the large-scale movement reveals that there are individual cycles constituting the bird's small-scale movements which are continually repeated. While the large-scale movement appears as a steady-state cruise-type motion horizontal to the Earth's surface (Fig. 3), the small-scale movements are of a pronounced three-dimensional and highly dynamic nature, yielding repetitive cycles (Fig. 4). They show distinct motions in the longitudinal, lateral and vertical directions. There are four flight phases, which are the characteristic elements of each cycle, denoted by numbers 1–4 at the first cycle: (1) windward climb; (2) upper curve from windward to leeward flight direction; (3) leeward descent; and (4) lower curve from leeward to windward flight direction. A flight cycle is the basic constituent of dynamic soaring.

Characteristics of dynamic soaring

Altitude, speed and total energy

A more detailed examination of dynamic soaring cycles yields the behaviour and magnitude of quantities relevant for this flight mode. With knowledge of these features, further characterization of dynamic soaring is possible. For this purpose, two cases were selected from the experimental data obtained in the in-flight measurements. These cases refer to the altitude interval that the bird traverses during dynamic soaring cycles, yielding cycles with a large or a small altitude interval (Figs 5 and 6, where Fig. 5 is the case already shown in Fig. 4). Selection of the altitude interval – instead of another quantity – is based on its importance for energy gain. This is because the greatest wind speed that the bird encounters in a dynamic soaring cycle is determinative for the achievable energy gain. The greatest wind speed is at the top of the altitude interval because the wind speed increases with altitude (Stull, 2003), i.e. with distance from the sea surface, where it is practically zero. With the altitude intervals selected for Figs 5 and 6, a wide range is covered, yielding representative results for dynamic soaring in albatrosses.

The altitude region extends from zero to about 15 m in the larger altitude interval case, and to less than 9 m in the small altitude interval one. Altitude and inertial speed (i.e. the speed related to

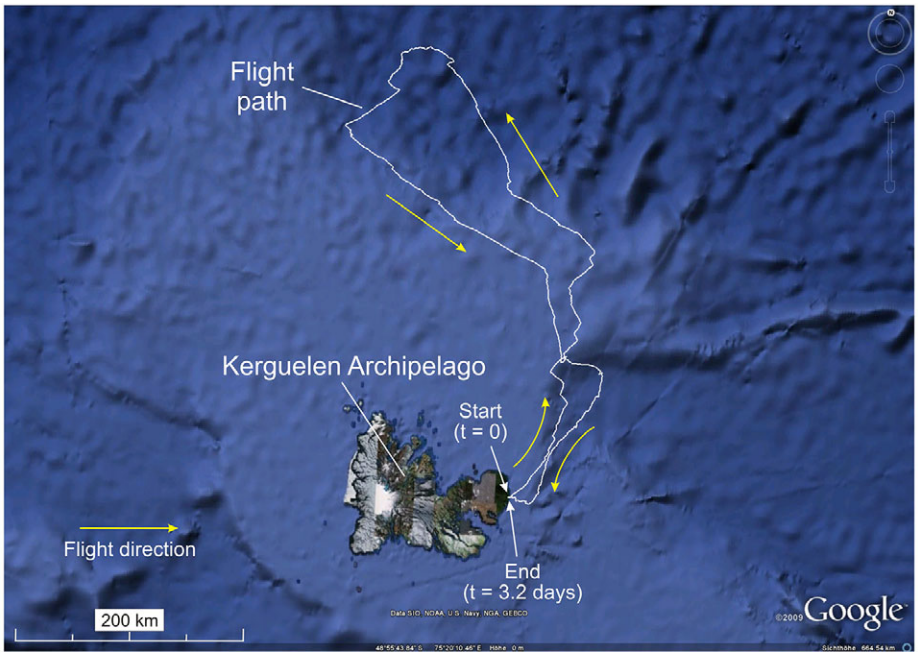

Fig. 3. Foraging trip of a wandering albatross: large-scale movement. The flight path of a long-distance foraging trip of a wandering albatross is shown (flight tracking duration: 3.2 days, data sampling rate: 10 Hz throughout the whole flight). The foraging trip begins (t=0) and ends (t=3.2 days) at the Kerguelen Archipelago. Its length is 1120 km. The flight path shows the movement of the bird on a large-scale basis, which is of a cruise-type steady-state nature. On this basis, the small-scale movements that comprise the large-scale movement are not visible. The small-scale movements, which are of a highly dynamic nature, are made up of dynamic soaring cycles. Map data: Google, SIO, NOAA, US Navy, NGA, GEBCO.

the Earth as an inertial reference system) show a cyclic behaviour such that they are continually repeated, with the speed lagging behind the altitude. The speed range run through during a cycle is greater in the larger altitude interval case, while the highest speed level, which is close to 30 m s^{-1}, is the same in the two cases. The duration of a cycle is of the order of 10 s, with somewhat greater values in the large altitude interval case and smaller values in the other.

Furthermore, the results of an energy analysis are presented in Figs 5 and 6, showing the total energy referenced to the weight:

$$\frac{E}{mg} = h + \frac{V_{\text{inert}}^2}{2g}, \quad (1)$$

where E is the total energy, m is the mass of the bird, g is the acceleration due to gravity, h is the altitude and V_{inert} is the inertial speed. The total energy made up of the sum of the potential and kinetic energy shows also a cyclic behaviour. Its higher levels are about $E/(mg)$=40 m for all cycles in both altitude interval cases while the lower levels differ.

There are characteristic properties concerning the energy gain in terms of the energy extraction from the shear wind and its transfer to the bird. The main point is the section of the dynamic soaring cycle where the energy gain is achieved. This is graphically illustrated in Figs 5 and 6 (indicated by the grey shading). The total energy begins to increase during the climb. At the top of the trajectory, the energy increase, being in full progress, continues. It comes to a stop in the course of the descent, after the altitude has already decreased. At this point, the total energy of the bird is at its maximum. There are large energy gains in all cycles, reaching as high as 300% of the value at beginning of a cycle (Fig. 5, first and third cycle). The way in which the energy gain is achieved holds for all cycles shown in Figs 5 and 6. Thus, it applies to the large altitude interval case as well as to the small interval case.

The energy diagrams in Figs 5 and 6 also show the kinetic and the potential energy. A comparison of the individual energy curves reveals that the increase in the total energy during the energy gain phase consists primarily of an increase in the kinetic energy, whereas the potential energy increase is significantly smaller. Thus, the total energy gain from the shear wind is mainly a kinetic energy gain. This means that, with regard to the motion of the bird, there is an increase in favour of speed when compared with altitude.

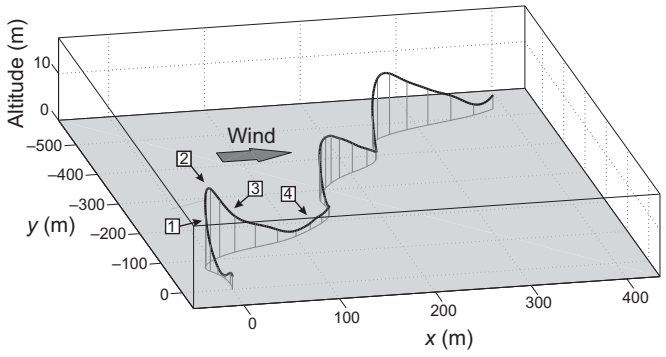

Fig. 4. Dynamic soaring cycles. A perspective view on dynamic soaring cycles is presented. The small-scale movements, which show distinct motions in the longitudinal, lateral and vertical directions, are made up of dynamic soaring cycles. As shown for the first cycle (indicated by nos. 1–4), a dynamic soaring cycle consists of (1) a windward climb, (2) a curve from windward to leeward at the upper altitude, (3) a leeward descent and (4) a curve from leeward to windward at low altitude close to the sea surface. This holds for all dynamic soaring cycles.

Upper curve: trajectory section of energy gain

For verification of dynamic soaring, the trajectory section in which the energy gain is achieved is determinative. This is made recognisable in Figs 7 and 8, with colour coding used to show the relationship between total energy and trajectory. The central issue is the trajectory section associated with the energy gain. The energy gain is achieved in the curve where the flight direction changes from windward to leeward, as indicated by the colour change from blue to red. Reference to Figs 5 and 6 reveals that this flight direction change occurs in the upper altitude region of each cycle, around the top of the trajectory. Thus, the curve in question where the change of flight direction from windward to leeward takes place is in the upper altitude region, yielding the upper curve of the dynamic

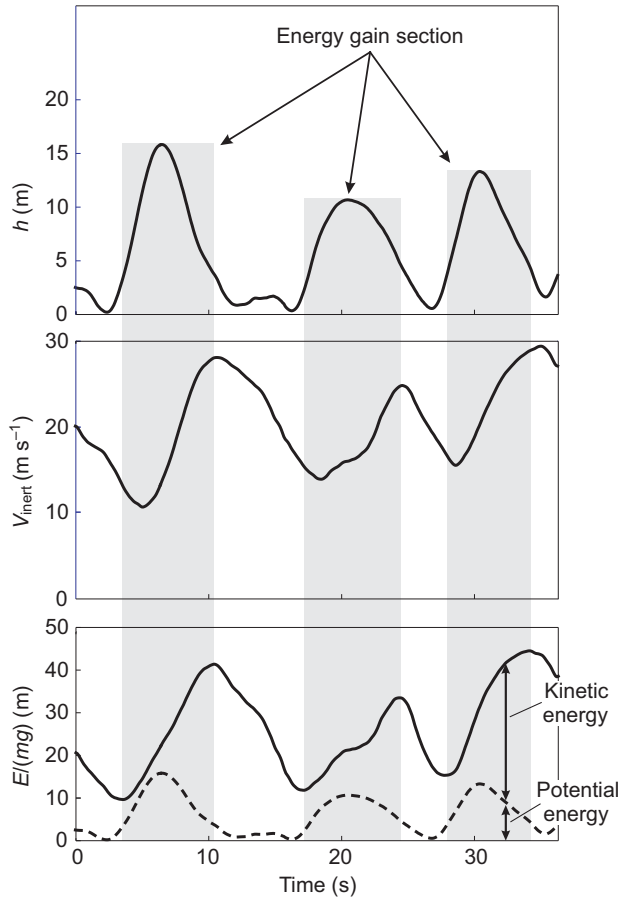

Fig. 5. Altitude, inertial speed and energy of dynamic soaring cycles with a large altitude interval. (These cycles are the dynamic soaring cycles presented in Fig. 4.) The altitude h shows a cyclic behaviour (between minimum at sea surface and maximum at the top of the trajectory). The inertial speed V_{inert}, which is also cyclic, has a time lag relative to the altitude with regard to its oscillatory behaviour. But it is increased already during the climb, despite the altitude increase. This indicates that there is a simultaneous increase of potential and kinetic energy to yield an increase of the total energy. The total energy, $E/(mg)=h+V_{inert}^2/(2g)$, begins to increase during the climb and reaches its maximum after the top of the trajectory has been passed. Thus, the energy gain is achieved around the top of the trajectory. The total energy curve is smooth and continuous. Hence, the extraction of energy from the shear wind is also smooth and continuous. There are no discontinuities or energy pulses. Furthermore, the kinetic energy and the potential energy are also shown in the total energy diagram.

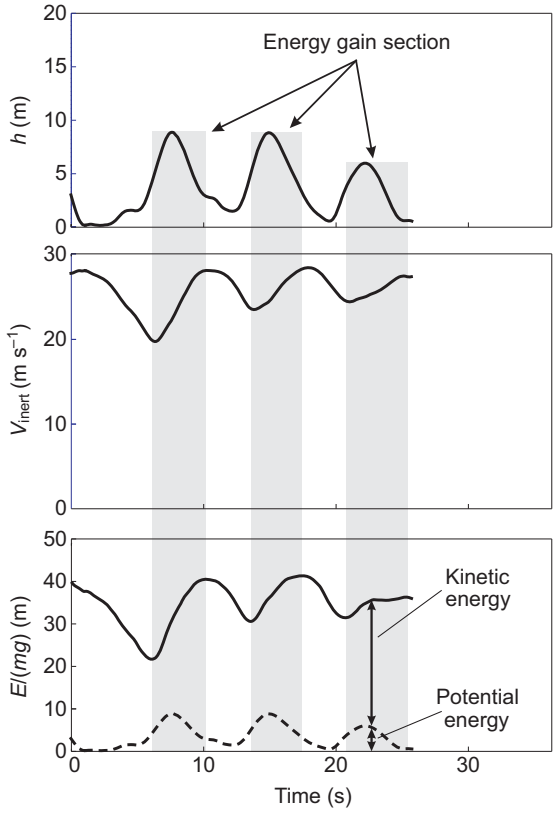

Fig. 6. Altitude, inertial speed and total energy of dynamic soaring cycles with a small altitude interval. The altitude intervals in this case are significantly smaller than those in Fig. 5. The upper speed level is of comparable magnitude, whereas the speed intervals between the maximum and minimum values are considerably smaller. Corresponding with the smaller altitude interval, the duration of a dynamic soaring cycle is shorter. An important result concerns the total energy behaviour when comparing the small and large altitude interval cases. It turns out that the level of the total energy is of equal magnitude in the two cases. The range between the maximum and minimum values differs. In the small altitude interval case, the potential energy level is reduced.

soaring cycle. The trajectory position at which the maximum total energy is reached is at the end of the upper curve. This holds for all cycles, in the large as well as in the small altitude interval cases. As a result, the upper curve can be qualified as the characteristic flight phase of dynamic soaring for achieving an energy gain.

The lower curve is the trajectory section where a total energy loss occurs (with red to blue change, Figs 7 and 8). This also holds for all cycles, in both the large as well as small altitude interval cases. As the wind speed is low here (Stull, 2003), the energy loss is not as large as it would be at a higher altitude. This is the reason why the curve where the flight direction changes from leeward to windward is in the lower altitude region, close to the sea surface.

Dynamic soaring cycles on a large-scale representation

In Figs 4–8, the decisive motion quantities and the energy balance essential for dynamic soaring as well as their relationship to the flight trajectory are presented so that the physical mechanism of the energy gain from the wind can be shown and identified as a unique characteristic of this flight mode. Supplementary to the small-scale movement representation, trajectory sections of greater length are depicted in Fig. 9 to illustrate how dynamic soaring manifests on a larger scale. Three wind cases are selected because of the essential significance of the wind for dynamic soaring, i.e. downwind flights at low and at high wind speed as well as upwind flight. Basically, all three trajectory sections show the typical pattern of dynamic soaring, which consists entirely of winding and curving segments.

The downwind flight cases at low and high wind speed are similar with regard to the extension of the curved segments in the longitudinal and lateral directions. Furthermore, the overall flight directions in both cases appear as a straight movement on a large-scale basis. Compared with this, the upwind case shows significant differences. Here, the extension of the curved segments in the longitudinal and lateral directions is much more pronounced. The overall flight direction is not so straight, being more of a meandering type. The individual segments are rather irregular, particularly in comparison with the downwind cases.

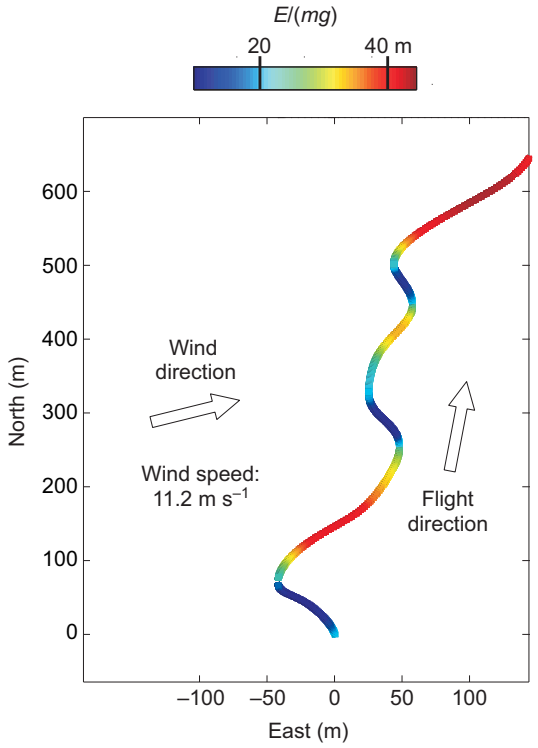

Fig. 7. Relationship between total energy and flight trajectory of dynamic soaring cycles with a large altitude interval (dynamic soaring cycles presented in Fig. 5). The total energy, $E/(mg)=h+V_{inert}^2/(2g)$, is indicated along the trajectory using colour coding. Quantification is possible with reference to the bar (at the top), which establishes a relationship between colour and total energy where the change from blue through green and yellow to red indicates the total energy increase from the lowest to the highest level. The colour changes from blue to red and, thus, the total energy increases in all curves where the flight direction is changed from windward to leeward. The total energy in each cycle is at its maximum after the upper curves have been completed. Thereafter, the colour changes from red to blue and, thus, the total energy decreases in all curves where the flight direction is changed from leeward to windward. These curves are at low altitude. The direction and the speed of the wind are also indicated in Fig. 7. The wind speed holds for 10 m altitude. The method for determining wind direction and speed is given in Materials and methods ('Wind determination').

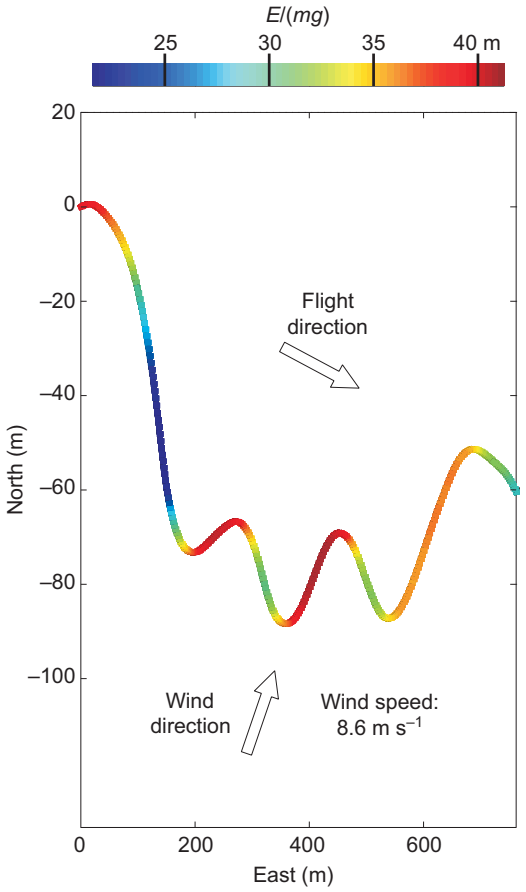

Fig. 8. Relationship between total energy and flight trajectory of dynamic soaring cycles with a small altitude interval (dynamic soaring cycles presented in Fig. 6). The relationship between total energy, dynamic soaring trajectory and wind direction is basically the same as in the large altitude case presented in Fig. 7. This particularly holds for the upper curve where the energy gain is achieved. In each cycle, the total energy is at its maximum after completion of the upper curves. Furthermore, the total energy decreases in all lower curves, where the flight direction is changed from leeward to windward. The direction and speed of the wind are also indicated in Fig. 8 (again for 10 m altitude).

Comparison with current theories and explanations for dynamic soaring

Theory of wind-gradient soaring

The theory of wind-gradient soaring is based on the wind gradient in the shear layer above the sea surface (Lighthill, 1975; Norberg, 1990; Spedding, 1992; Tickell, 2000; Dhawan, 2002; Lindhe Norberg, 2004; Azuma, 2006; Denny, 2009). According to this theory, energy can be obtained by climbing against the wind because the wind speed increases as a result of the wind gradient. Analogously, an energy gain is considered to be possible when descending in a leeward direction. For a climb without loss in airspeed, the minimally required wind gradient is given by the following expression (e.g. Pennycuick, 2002):

$$(\mathrm{d}V_\mathrm{W}/\mathrm{d}h)_\mathrm{required} = g/V\,, \qquad (2\mathrm{A})$$

yielding, for an airspeed of V=15 m s^{-1}:

$$(\mathrm{d}V_\mathrm{W}/\mathrm{d}h)_\mathrm{required} = 0.7\ \mathrm{s}^{-1}\,. \qquad (2\mathrm{B})$$

In Figs 5 and 6, it is shown that the increase of the total energy takes place in the upper altitude region. In that region, the wind speed shows only minor changes with altitude so that the wind gradient is very small. This was confirmed by an analysis of the wind speed and the wind gradient using wind measurement data (Perry, 2001; Müller, 2009) and a logarithmic wind model (Stull, 2003). The analysis yields an average effective wind gradient of:

$$(\mathrm{d}V_\mathrm{W}/\mathrm{d}h)_\mathrm{av} = 0.1\ \mathrm{s}^{-1}\,, \qquad (3)$$

for the altitude region in mind. A comparison of $(\mathrm{d}V_\mathrm{W}/\mathrm{d}h)_\mathrm{av}$=0.1 s^{-1} with $(\mathrm{d}V_\mathrm{W}/\mathrm{d}h)_\mathrm{required}$=0.7 s^{-1} shows that the existing wind gradient is far too small when compared with the required value. This means with regard to the theory of wind-gradient soaring that the wind gradient itself is insignificant for the energy gain. Rather, the energy gain is due to the change in the flight direction from windward to leeward in the upper curve.

Theory of gust soaring

The theory of gust soaring is concerned with discontinuities in the wind flow (Pennycuick, 2002; Pennycuick, 2008; Suryan et al., 2008; Langelaan, 2008; Langelaan and Bramesfeld, 2008). According to this theory, there is an alternative flight mode by which

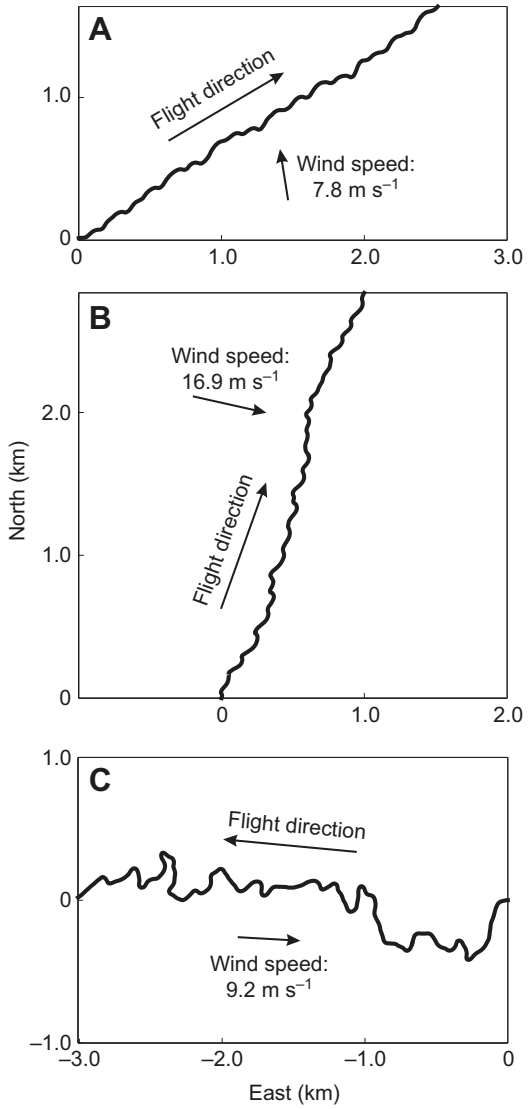

Fig. 9. In-flight measurements of large-scale movements. Large-scale movements are presented for three wind cases. In each case, the large-scale movement consists completely of dynamic soaring cycles which are continually repeated. The curving segments are connected to each other without any straight part in between. (A) Downwind flight at low wind speed; (B) downwind flight at high wind speed; and (C) upwind flight.

pulses of energy are obtained from a flight through the separated air flow region behind wave crests. It implies that this happens at low level.

Investigation of the energy behaviour (Figs 5 and 6) shows that all total energy curves are continuous and smooth. This means with regard to the theory of gust soaring that there are no discontinuities and no energy pulses, but there is a continuous extraction of energy from the shear wind to the bird. Furthermore, the energy gain is not attained at low level. Rather, it is achieved in the upper altitude region, around the top of the trajectory.

This conclusion is further confirmed by data from the flight of an albatross over flat land. In Fig. 10, the trajectory obtained from in-flight measurement of an albatross flying over land is presented. The flight over land consists completely of dynamic soaring cycles, without any straight trajectory portion in between. All cycles show the characteristic pattern of dynamic soaring. The elevation of the terrain in the area of the dynamic soaring trajectory over land is presented in Fig. 11, revealing how flat this area is. Because of the flatness of the land, separated air flow is not possible. As a result, there cannot be an effect such as energy pulses obtained from flight through a separated air flow region. Rather, the energy gain is achieved in a continuous and smooth manner in the upper curve of dynamic soaring.

Wave soaring and wave lift

Wave soaring and wave lift are considered to be a possible source of energy gain (Berger and Göhde, 1965; Wilson, 1975; Pennycuick, 1982; Sheng et al., 2005; Richardson, 2011). By flying along the flanks of waves, the birds can make use of rising air currents directly related to the waves. This would imply flight at low altitude, close to the waves.

The dynamic soaring cycles over flat land, as shown in Figs 10 and 11, provide evidence for another energy transfer mechanism. As the ground is flat there are no geometric forms similar to waves. Thus, no rising air currents exist that may be used for achieving an energy gain. Instead, there is only horizontal wind. This means that the energy is extracted from horizontally moving air rather than from rising air currents.

Furthermore, wave soaring and wave lift would show flight segments close to the water surface where altitude and speed are constant or slowly changing. However, this is not the case, as may be seen in Figs 4–7. Rather, the energy gain is achieved in the upper altitude region where the effect of waves on air currents can be assumed to be negligible, if not zero. As a result, this effect plays no role in energy gain.

Aerodynamic ground effect

The aerodynamic ground effect yields a decrease of the drag when a bird is close to the water surface (Blake, 1983; Hainsworth, 1988; Norberg, 1990; Rayner, 1991). It rapidly reduces with the distance from the ground. The aerodynamic ground effect has an influence only during flight at low level. It yields a decrease of the induced drag factor by about 10% at a distance of a wing semispan from the ground, with less of a decrease for larger distances (Rayner, 1991). Flight involving a high bank angle, as is the case in the lower curve of dynamic soaring of albatrosses, suggests that the effectiveness of the aerodynamic ground effect would be reduced.

A main point in this context is that the aerodynamic ground effect cannot increase the total energy because it merely reduces the aerodynamic drag so that there is still a dissipative effect of the drag. As a result, the aerodynamic ground effect plays no role in the energy gain.

Energy gain mechanism in dynamic soaring: propulsive force due to the wind

A deeper insight into the physical mechanism underlying the energy gain in dynamic soaring is possible with an analysis of the force effecting this gain. There is a propulsive force that acts at the bird and yields an increase of the total energy. The generation of this force is shown in Fig. 12.

Fig. 12A shows the lift vector, as seen from behind in direction of the airspeed vector. The lift vector $\vec{L}$ can be decomposed into two components: $\vec{L}_{V1}$ and $\vec{L}_{V2}$. The component $\vec{L}_{V1}$ is in the plane of the speed vectors, while the component $\vec{L}_{V2}$ is perpendicular to that plane. This means that $\vec{L}_{V1}$ is doing work and, thus, exerts an effect on the total energy. By contrast, $\vec{L}_{V2}$ is doing no work so it has no effect on the total energy.

Fig. 12B shows the lift and drag vectors, as seen from above on the plane of the speed vectors. Thus, the force $\vec{L}_{V1}$ and the drag vector

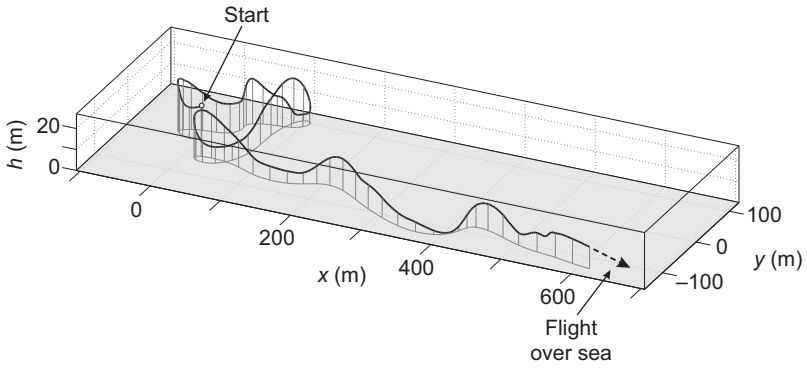

Fig. 10. View of dynamic soaring cycles over land. The coordinate system is referenced to the starting point of the dynamic soaring trajectory (denoted by x=0, y=0). The solid line represents the flight path over land, and the dashed arrow indicates the beginning of the flight over the sea. The bird performs a number of consecutive dynamic soaring cycles over land before it reaches the sea. The extension of the dynamic soaring cycles in the vertical as well as the longitudinal and lateral directions is of the same magnitude as the cycles recorded in in-flight measurements over the sea (as, for example, shown in Fig. 4).

$\vec{D}$ can be made visible. It is shown that $\vec{L}_{V1}$ has a component $\vec{L}_{V1}\sin\alpha_W$ acting in the direction of the inertial speed vector $\vec{V}_{inert}$ which determines the motion of the bird with respect to the Earth (used as an inertial reference system). This means that the component $\vec{L}_{V1}\sin\alpha_W$ exerts a propulsive effect on the bird, being equivalent to a thrust propelling the bird. Therefore, it may be named propulsive force:

$$F_{propulsive} = L_{V1}\sin\alpha_W . \quad (4)$$

As $F_{propulsive}$ is doing work, it has an effect on the total energy state of the bird. To show this, reference is made to the relationship between the total energy E and the work done by the forces acting at the bird along the flight path. These forces are the components of the lift and the drag vectors parallel to the inertial speed vector: $F_{propulsive}=L_{V1}\sin\alpha_W$ and $D\cos\alpha_W$ (Fig. 12B). The relationship between the total energy E and the work done by the described forces can be formulated as (with t and τ denoting time quantities):

$$E(t) - E(t_0) = \int_{t_0}^{t} (F_{propulsive} - D\cos\alpha_W)V_{inert}\,d\tau . \quad (5)$$

Differentiation with regard to the time results in the following relation:

$$\dot{E} = (F_{propulsive} - D\cos\alpha_W)V_{inert} . \quad (6)$$

Solving for $F_{propulsive}$ yields:

$$F_{propulsive} = \frac{\dot{E}}{V_{inert}} + D\cos\alpha_W . \quad (7)$$

From an analysis of $F_{propulsive}$ using data from the albatrosses' in-flight measurements, the results presented in Fig. 13 are obtained. These results basically show: (1) $F_{propulsive}$ is the force that generates the total energy gain; this takes place in the upper curve; and (2) the effect of $F_{propulsive}$ is very strong.

Positive $F_{propulsive}$ values mean that energy is extracted from the shear wind and transferred to the bird, yielding a total energy gain, while negative $F_{propulsive}$ values cause an energy loss. The range of positive $F_{propulsive}$ values is associated with the upper curve, as indicated in Fig. 13 by the grey shading. The fact that $F_{propulsive}$ reaches its greatest level around the middle of the upper curve means that it is most effective in the higher altitude region of the dynamic soaring cycle. This again verifies that the upper curve is the characteristic flight phase of dynamic soaring for achieving an energy gain.

As the lift vector is proportional to the airspeed squared, yielding:

$$L = C_L(\rho/2)V^2S , \quad (8)$$

the following relation holds for the propulsive force:

$$F_{propulsive} \sim V^2\sin\alpha_W . \quad (9)$$

This relation shows that a large value of $\vec{V}$ and a wide angle α_W between $\vec{V}_{inert}$ and $\vec{V}$ increase the propulsive effect of $F_{propulsive}$. The speed vector relationship presented in Fig. 12B shows that the angle α_W is wide when $\vec{V}_W$ is large and highly inclined with regard to $\vec{V}_{inert}$. Large values of α_W and $\vec{V}_{inert}$ also contribute to large $\vec{V}$ values. This is evidence for the significance of the upper curve for dynamic soaring because here the wind speed takes on the largest values during the entire cycle and the angle α_W is wide.

The total energy management in the dynamic soaring cycle is dominated by $F_{propulsive}$. This is confirmed by a comparison with the contribution of the drag, which is the only other force doing

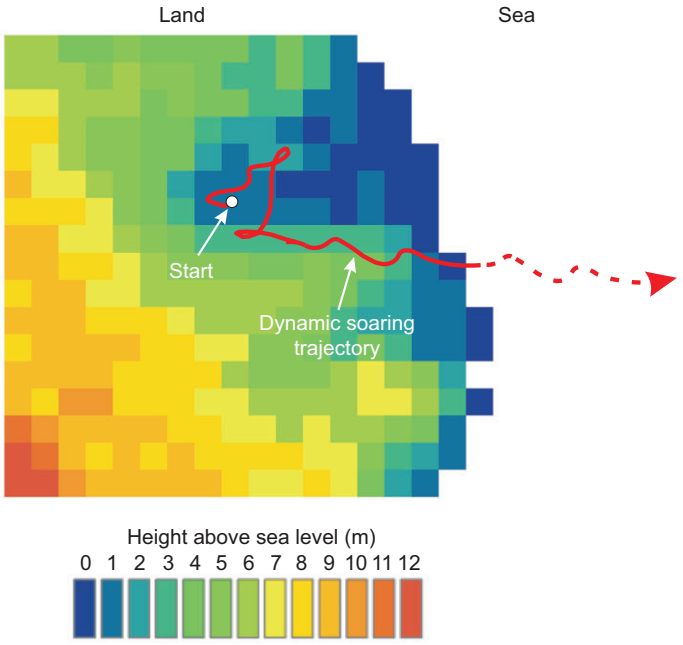

Fig. 11. Terrain elevation in an area where dynamic soaring cycles over land were performed, obtained using the SRTM digital elevation model (Jarvis et al., 2008). The SRTM model provides a grid consisting of rectangular elements of about 90×90 m size for the Kerguelen area. Coloured bars below the terrain image indicate the altitude above sea level. The ground track of the dynamic soaring cycles shown in Fig. 10 is also presented. The area is in the land sector of the Kerguelen Archipelago depicted in Fig. 3 where the albatross foraging trip began and ended. Referencing the dynamic soaring trajectory to the terrain elevation shows that the flight was performed over flat land. According to the grid element colouring along the dynamic soaring trajectory, there are no hills or geometric forms similar to waves. Thus, there cannot be such effects as a separated air flow region behind wave crests or rising air currents related to waves.

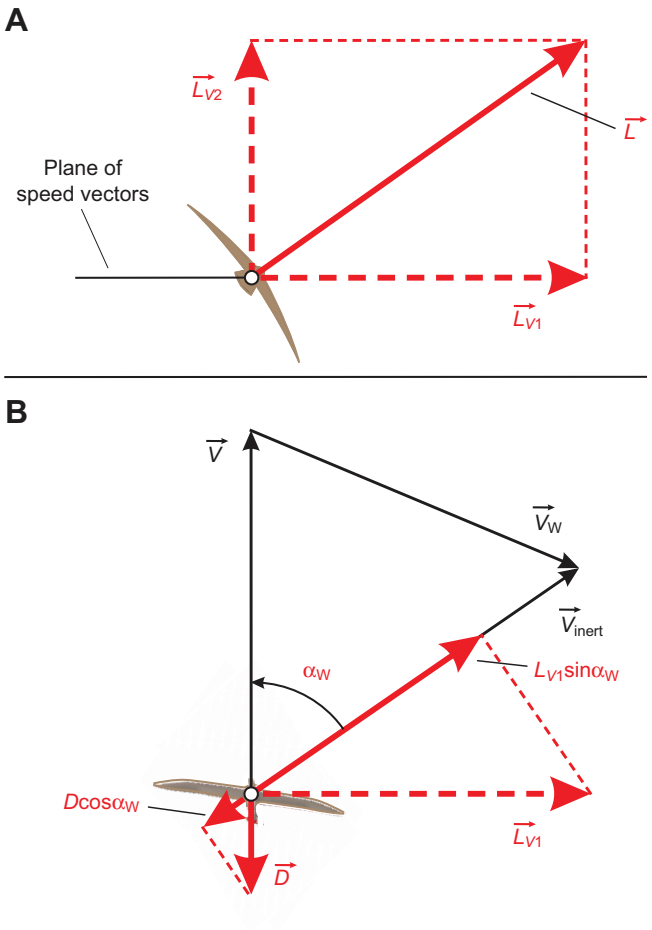

Fig. 12. Force and speed vector diagram. (A) View of the bird seen from behind in the direction of the airspeed vector $\vec{V}$. The lift vector denoted by $\vec{L}$ is perpendicular to the wings of the bird. It can be decomposed into a component $\vec{L}_{V1}$ in the plane made up by the speed vectors $\vec{V}_{inert}$, $\vec{V}$ and $\vec{V}_W$ (appearing as a line), and into a component $\vec{L}_{V2}$ perpendicular to that plane. The plane made up by the speed vectors $\vec{V}_{inert}$, $\vec{V}$ and $\vec{V}_W$ has no fixed relationship to the horizontal, but is continually changing according to the motion of the bird in the course of the dynamic soaring flight manoeuvre. (B) View on the plane of the speed vectors: the inertial speed vector $\vec{V}_{inert}$, which describes the motion of the bird with respect to the Earth used as an inertial reference system; the airspeed vector $\vec{V}$, which describes the motion with respect to the moving air in the shear wind; and the wind speed vector $\vec{V}_W$. Furthermore, the lift vector component $\vec{L}_{V1}$, the drag vector $\vec{D}$ and the angle α_W are presented. The angle α_W describes the inclination of the airspeed vector $\vec{V}$ relative to the inertial speed vector $\vec{V}_{inert}$. There is an inclination ($\alpha_W \neq 0$) if the wind speed vector $\vec{V}_W$ is not parallel to but instead inclined relative to the inertial speed vector $\vec{V}_{inert}$. The angle α_W can be determined using the relationship between the speed vectors $\vec{V}_{inert}$ and $\vec{V}_W$, which are known from the GPS logger in-flight measurements and the QuikSCAT wind data (as described in Materials and methods, 'Wind determination'). The lift vector component $\vec{L}_{V1}$ is, by definition, orthogonal to the airspeed vector $\vec{V}$. Because of the inclination of $\vec{V}$ relative to $\vec{V}_{inert}$ by the angle α_W, $\vec{L}_{V1}$ has a component $\vec{L}_{V1}\sin\alpha_W$ parallel to the inertial speed vector $\vec{V}_{inert}$. This component is effective in terms of a propulsive force $F_{propulsive}=L_{V1}\sin\alpha_W$. As a result, the work done by $F_{propulsive}=L_{V1}\sin\alpha_W$ yields an increase in the total energy. The drag vector $\vec{D}$ exerts a dissipative effect concerning the energy, producing a negative work due to its component $D\cos\alpha_W$ acting in the negative direction of $\vec{V}_{inert}$. The component $\vec{L}_{V1}\sin\alpha_W$ and, thus, its propulsive effect, is large when there is a wide angle α_W between $\vec{V}_{inert}$ and $\vec{V}$. The angle α_W is wide when $\vec{V}_W$ is large and highly inclined with regard to $\vec{V}_{inert}$, as in B. In the upper curve, the wind speed $\vec{V}_W$ takes on the largest values during the entire cycle and the angle α_W is wide. This is evidence for the significance of the upper curve for dynamic soaring as that phase where the energy gain is achieved.

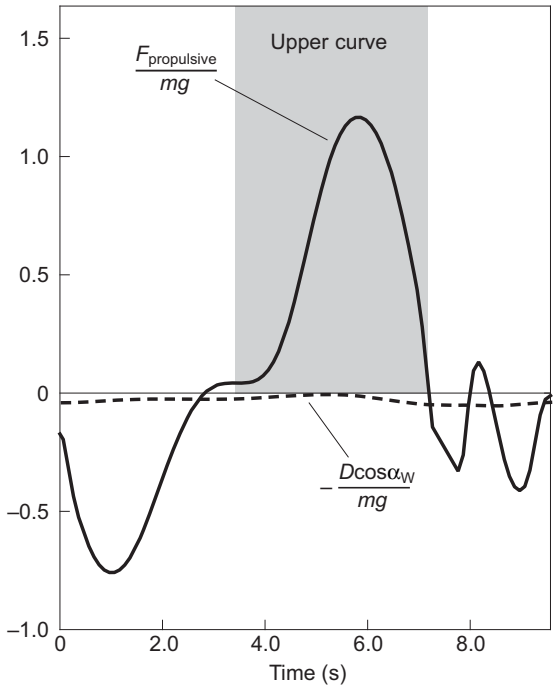

Fig. 13. Time histories of the forces doing work, $F_{propulsive}$ and $D\cos\alpha_W$. The propulsive force $F_{propulsive}$ shows positive and negative values. Where $F_{propulsive}$ is positive, the total energy of the bird is increased, yielding an energy gain. This part is associated with the upper curve, as indicated on the diagram using grey shading. Here, $F_{propulsive}$ reaches its highest level, yielding a maximum as large as $F_{propulsive,max} \approx 1.2mg$. In the negative $F_{propulsive}$ part, there is a total energy loss. This occurs in the lower curve. The drag component doing work, $D\cos\alpha_W$, yields a dissipative effect concerning the total energy (indicated by the minus sign). $D\cos\alpha_W$ is very small when compared with $F_{propulsive}$. As a result, the total energy behaviour is dominated by $F_{propulsive}$.

work and influencing the total energy. The analysis of the force relationship using data from the albatrosses' in-flight measurements is also concerned with the drag, yielding an estimation of its component $D\cos\alpha_W$, which is the drag component effective in doing work (Fig. 12B). In Fig. 13, the component $D\cos\alpha_W$ is also shown (the negative of $D\cos\alpha_W$ is selected because of its dissipative effect concerning the energy). Comparison with $F_{propulsive}$ reveals that $D\cos\alpha_W$ is substantially smaller. This particularly holds for the upper curve, where $D\cos\alpha_W$ is practically negligible. Thus, the total energy behaviour is influenced by the drag to a very small extent only, but dominated by $F_{propulsive}$.

A comparison with the force characteristics in the lower curve further deepens the insight into the energy management during dynamic soaring. In Fig. 14, the lift vector in the lower curve is presented, as seen from above on the plane of the speed vectors. The lift component $\vec{L}_{V1}\sin\alpha_W$ is now acting in the opposite direction to the inertial speed vector $\vec{V}_{inert}$. Thus, it yields a decrease of the total energy. However, there is an effect that reduces the size of $\vec{L}_{V1}\sin\alpha_W$. This is basically due to the wind speed being small at the altitude of the lower curve. As a result, the angle α_W is also small, yielding a reduction of $\vec{L}_{V1}\sin\alpha_W$. In Fig. 14, it is assumed for comparison purposes that the same size applies for $\vec{L}_{V1}$ and for the wind direction as in Fig. 12B, while the wind speed V_W is smaller because of the lower altitude. Comparison of Fig. 12B and Fig. 14 reveals that $\vec{L}_{V1}\sin\alpha_W$ differs considerably in the two cases, showing a significantly smaller value in the lower curve. This is an indication that the energy loss in the lower curve is smaller than the energy gain in the upper

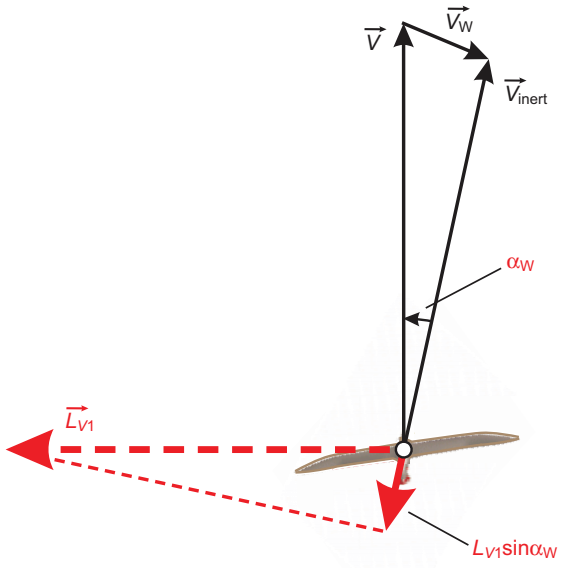

Fig. 14. A view on the plane of the speed vectors in the lower curve is presented, showing the lift vector components $\vec{L}_{V1}$ and $\vec{L}_{V1}\sin\alpha_W$ as well as the speed vectors $\vec{V}_{inert}$, $\vec{V}$ and $\vec{V}_W$. (The drag vector $\vec{D}$ and its component $\vec{D}\cos\alpha_W$ are not shown to maintain pictorial clarity.) In the lower curve, the lift component $\vec{L}_{V1}$ effectuates a curvature of the trajectory in such a way that the flight direction is changed from leeward to windward. This implies that its component $\vec{L}_{V1}\sin\alpha_W$ acts in the opposite direction to the inertial speed vector $\vec{V}_{inert}$. As the wind speed is small in the lower curve, the angle α_W is reduced. This yields a reduction of $\vec{L}_{V1}\sin\alpha_W$.

curve so that there is a net energy gain for the complete dynamic soaring cycle with regard to the effect of $F_{propulsive}$. The described force difference is confirmed by the time history of $F_{propulsive}$ depicted in Fig. 13, where the level of the negative values is smaller than that of the positive values.

Evidence of non-flapping in dynamic soaring

The results presented in Fig. 13 provide evidence that there is no wing flapping in dynamic soaring. Rather, the bird is in a gliding condition where the wings are held motionless and in a fixed position. Evidence for non-flapping is substantiated in the following.

As shown in Fig. 13, the propulsive force $F_{propulsive}$ approaches values as high as 120% of the weight so that it is larger than the weight of the bird, yielding a maximum propulsive force:

$$F_{propulsive,max} \approx 1.2\,mg\,. \quad (10)$$

A propulsive force this high cannot be generated by wing flapping. This is because for large birds like wandering albatrosses with a mass of about 10 kg the maximum propulsive force possible with wing flapping is smaller by an order of magnitude.

For estimating the maximum propulsive force possible with wing flapping, reference is made to scaling considerations published previously (Pennycuick, 2008). For this purpose, the following scaling relationships are assumed to apply: (1) the available power ($P_{available}$) generated by the flight muscles increases with mass according to $P_{available} \propto m^{5/6}$; (2) the minimum power required for airborne flight ($P_{required}$) increases with mass according to $P_{required} \propto m^{7/6}$; (3) the mass limit for birds capable of powered horizontal flight is around 16 kg. From these assumptions it follows that for a bird of 10 kg mass the estimated surplus of the available power over the required power is given by:

$$P_{available} \approx 1.2\,P_{required}\,. \quad (11)$$

The general thrust–power relationship in airborne flight yields for the propulsive force due to wing flapping:

$$F_{flapping} = \frac{P}{V}\,. \quad (12)$$

The flight condition at the minimum power required can be described by (Brüning et al., 2006):

$$P_{required} = \frac{2}{\sqrt[4]{27}}\left(\frac{C_D}{C_L}\right)_{min} mgV^*$$

$$V_{P_{required}} = \frac{V^*}{\sqrt[4]{3}}\,, \quad (13)$$

where $V_{P_{required}}$ is the speed at the minimum power required and V^* the speed at the minimum drag-to-lift ratio $(C_D/C_L)_{min}$. Using the relations described in Eqns 11–13, the following result is obtained for the maximum propulsive force due to wing flapping for a bird of 10 kg mass:

$$F_{flapping,max} \approx 1.4\left(\frac{C_D}{C_L}\right)_{min} mg\,. \quad (14)$$

For albatrosses, data from various sources for the possible range of minimum drag-to-lift ratios are available (Sachs, 2005), yielding a range of:

$$\left(\frac{C_D}{C_L}\right)_{min} = 0.04 - 0.05\,. \quad (15)$$

Applying $(C_D/C_L)_{min}=0.045$ as an average, the maximum propulsive force possible with wing flapping is:

$$F_{flapping,max} \approx 0.06\,mg\,. \quad (16)$$

This is smaller by an order of magnitude when compared with the maximum propulsive force in dynamic soaring $F_{propulsive,max} \approx 1.2mg$. As a result, the energy gain in dynamic soaring cannot be achieved by wing flapping. Rather, there is another mechanism which is due $F_{propulsive}$, as described in the preceding section.

The existence of a propulsive force this high ($F_{propulsive,max} \approx 1.2mg$ as opposed to $F_{flapping,max} \approx 0.06mg$) is evidence of the fact that dynamic soaring is performed without flapping the wings. Instead, the wings are kept in a fixed position, and hence in the position of soaring.

LIST OF SYMBOLS AND ABBREVIATIONS

C_D	drag coefficient
C_L	lift coefficient
$\vec{D}$	drag vector
E	total energy
$F_{flapping}$	propulsive force due to flapping
$F_{propulsive}$	propulsive force
g	acceleration due to gravity
h	altitude
$\vec{L}$	lift vector
$\vec{L}_{V1}$	lift vector component in speed vector plane
$\vec{L}_{V2}$	lift vector component perpendicular to speed vector plane
m	mass
$P_{available}$	available power
$P_{required}$	required power
S	wing reference area
t	time
t_b	arbitrary time base (1–3)
t_j	current time
V	airspeed

V^*	speed at the minimum drag-to-lift ratio, $(C_D/C_L)_{min}$
V_{inert}	inertial speed
$V_{Prequired}$	speed at minimum power required
V_W	wind speed
x	longitudinal coordinate
y	lateral coordinate
α_W	wind angle
Δ	bias
ρ	air density
τ	time

ACKNOWLEDGEMENTS

The authors thank J. Mardon for his help in the preliminary trials of the study, and Giacomo Dell'Omo, Wolfgang Heidrich, Franz Kümmeth and Alexei L. Vyssotski for contributing to technical tools as well as for conducting performance tests and optimizing the equipment.

AUTHOR CONTRIBUTIONS

Conception: G.S. Design: G.S., J.T. and F.B. Execution: J.T. and A.P.N. Interpretation of the findings: G.S. and J.T. Drafting and revising the article: G.S. and J.T.

COMPETING INTERESTS

No competing interests declared.

FUNDING

The authors are grateful to the Institut Polaire Français Paul Emile Victor, which supported this work (IPEV, Program No. 354) – the work was performed according to guidelines established by IPEV and CNRS for the Ethical Treatment of Animals. The authors are also grateful for the support provided by National Science Foundation International Research Fellowship for A.P.N. (no. 0700939).

REFERENCES

Azuma, A. (2006). *The Biokinetics of Flying and Swimming*, 2nd edn. Reston, VA: American Institute of Aeronautics and Astronautics, Inc.

Berger, M. and Göhde, W. (1965). Zur Theorie des Segelfluges von Vögeln über dem Meere. *Zool. Jb. Physiol.* **71**, 217-224.

Blake, R. W. (1983). Mechanics of gliding in birds with special reference to the influence of the ground effect. *J. Biomech.* **16**, 649-654.

Bonadonna, F., Bajzak, C., Benhamou, S., Igloi, K., Jouventin, P., Lipp, H. P. and Dell'Omo, G. (2005). Orientation in the wandering albatross: interfering with magnetic perception does not affect orientation performance. *Proc. Biol. Sci.* **272**, 489-495.

Brüning, G., Hafer, X. and Sachs, G. (2006). *Flugleistungen*, 4th edn. Berlin: Springer-Verlag.

Catry, P., Phillips, R. A. and Croxall, J. P. (2004). Sustained fast travel by a grey-headed albatross (*Thalassarchie chrysostoma*) riding an Antarctic storm. *Auk* **121**, 1208-1213.

Croxall, J. P., Silk, J. R. D., Phillips, R. A., Afanasyev, V. and Briggs, D. R. (2005). Global circumnavigations: tracking year-round ranges of nonbreeding albatrosses. *Science* **307**, 249-250.

Denny, M. (2009). Dynamic soaring: aerodynamics for albatrosses. *Eur. J. Phys.* **30**, 75-84.

Dhawan, S. (2002). *How Birds Fly*. India: National Book Trust. ISBN 81-237-3738-6.

Hainsworth, F. R. (1988). Induced drag savings from ground effect and formation flight in brown pelicans. *J. Exp. Biol.* **135**, 431-444.

Jarvis, A., Reuter, H. I., Nelson, A. and Guevara, E. (2008). *Hole-filled Seamless SRTM Data V4*. International Centre for Tropical Agriculture (CIAT). http://srtm.csi.cgiar.org.

Jouventin, P. and Weimerskirch, H. (1990). Satellite tracking of wandering albatrosses. *Nature* **343**, 746-748.

Langelaan, J. W. (2008). *Biologically Inspired Flight Techniques for Small and Micro Unmanned Aerial Vehicles*. American Institute of Aeronautics and Astronautics, AIAA 2008-6511.

Langelaan, J. W. and Bramesfeld, G. (2008). *Gust Energy Extraction for Mini- and Micro-Uninhabited Aerial Vehicles*. American Institute of Aeronautics and Astronautics, AIAA 2008-223.

Lighthill, M. J. (1975). Aerodynamic aspects of animal flight. In *Swimming and Flying in Nature*, Vol. 2 (ed. T. Y. Wu, C. J. Brokaw and C. Brennen), pp. 423-491. New York, NY: Plenum Press.

Lindhe Norberg, U. M. (2004). Bird flight. *Acta Zoologica Sinica* **59**, 921-935.

Müller, H. (2009). *QuikSCAT L3 Global Wind Data – Projection on Local Flight Trajectories and 3D Interactive Visualization*. Seminar paper, Institute of Flight System Dynamics, Technische Universität München.

Norberg, U. M. (1990). *Vertebrate Flight*. Berlin: Springer-Verlag.

Pennycuick, C. J. (1982). The flight of petrels and albatrosses (Procellariiformes), observed in South Georgia and its vicinity. *Philos. Trans. R. Soc. B* **300**, 75-106.

Pennycuick, C. J. (2002). Gust soaring as a basis for the flight of petrels and albatrosses (Procellariiformes). *Avian Science* **2**, 1-12.

Pennycuick, C. J. (2008). *Modelling the Flying Bird*. Elsevier, Academic Press. ISBN: 978-0-12-374299-5.

Perry, K. L. (2001). SeaWinds on QuikSCAT Level 3 Daily, Gridded Ocean Wind Vectors (JPL SeaWinds Project). Version 1.1. JPL Document D-20335, Jet Propulsion Laboratory, Pasadena, CA.

Phillips, R. A., Xavier, J. C. and Croxall, J. P. (2003). Effects of satellite transmitters on albatrosses and petrels. *Auk* **120**, 1082-1090.

Rayner, J. M. V. (1991). On the aerodynamics of animal flight in ground effect. *Philos. Trans. R. Soc. B* **334**, 119-128.

Richardson, P. L. (2011). How do albatrosses fly around the world without flapping their wings? *Prog. Oceanogr.* **88**, 46-58.

Sachs, G. (2005). Minimum shear wind strength required for dynamic soaring of albatrosses. *Ibis* **147**, 1-10.

Sachs, G., Traugott, J., Nesterova, A. P., Dell'Omo, G., Kümmeth, F., Heidrich, W., Vyssotski, A. L. and Bonadonna, F. (2012). Flying at no mechanical energy cost: disclosing the secret of wandering albatrosses. *PLoS ONE* **7**, e41449.

Sheng, Q., Wu, D. and Zhang, L. (2005). Aerodynamic forces acting on an albatross flying above sea-waves. *Appl. Math. Mech.* **26**, 1222-1229.

Spedding, G. R. (1992). The aerodynamics of flight. In *Advances in Comparative and Environmental Physiology*: *Mechanics of Animal Locomotion*, Vol. 11, pp. 51-111. Berlin: Springer-Verlag.

Stull, R. B. (2003). *An Introduction to Boundary Layer Meteorology*. Dordrecht: Kluwer Academic Publishers.

Suryan, R. M., Anderson, D. J., Shaffer, S. A., Roby, D. D., Tremblay, Y., Costa, D. P., Sievert, P. R., Sato, F., Ozaki, K., Balogh, G. R. et al. (2008). Wind, waves, and wing loading: morphological specialization may limit range expansion of endangered albatrosses. *PLoS ONE* **3**, e4016.

Tickell, W.L.N. (2000). *Albatrosses*. Robertsbridge: Pica Press.

Traugott, J., Dell'Omo, G., Vyssotski, A. L., Odijk, D. and Sachs, G. (2008a). A time-relative approach for precise positioning with a miniaturized L1 GPS logger. In *Proceedings of the 21st International Technical Meeting of the Satellite Division of the Institute of Navigation ION GNSS 2008*, 16-19 September 2008, pp. 1883-1894. Savannah, GA, USA.

Traugott, J., Odijk, D., Montenbruck, O., Sachs G., and Tiberius, Chr. (2008b). Making a difference with GPS – time differences for kinematic positioning with low-cost receivers. *GPS World* **19**, 48-52, 54, 57.

Weimerskirch, H., Guionnet, T., Martin, J., Shaffer, S. A. and Costa, D. P. (2000). Fast and fuel efficient? Optimal use of wind by flying albatrosses. *Proc. Biol. Sci.* **267**, 1869-1874.

Weimerskirch, H., Bonadonna, F., Bailleul, F., Mabille, G., Dell'Omo, G. and Lipp, H.-P. (2002). GPS tracking of foraging albatrosses. *Science* **295**, 1259.

Wilson, J. A. (1975). Sweeping flight and soaring by albatrosses. *Nature* **257**, 307-308.

Wilson, R. P., Putz, K., Peters, G., Culik, B., Scolaro, J. A., Charrassin, J.-B. and Ropert-Coudert, Y. (1997). Long-term attachment of transmitting and recording devices to penguins and other seabirds. *Wildl. Soc. Bull.* **25**, 101-106.